micromachines

MDPI

Article

A Sub-1 Hz Resonance Frequency Resonator Enabled by Multi-Step Tuning for Micro-Seismometer

Jun Wu [1], Hideyuki Maekoba [2], Arnaud Parent [2] and Tamio Ikehashi [1,*]

[1] Graduate School of Information Production and Systems, Waseda University, Kitakyushu-shi 808-0135, Japan; woojun@fuji.waseda.jp
[2] Coventor, A Lam Research Company, Fremont, CA 94538, USA; Hideyuki.Maekoba@lamresearch.com (H.M.); aparent@coventor.com (A.P.)
* Correspondence: t.ikehashi@waseda.jp

Abstract: We propose a sub-1 Hz resonance frequency MEMS resonator that can be used for seismometers. The low resonance frequency is achieved by an electrically tunable spring with an ultra-small spring constant. Generally, it is difficult to electrically fine-tune the resonance frequency at a near-zero spring constant because the frequency shift per voltage will diverge at the limit of zero spring constant. To circumvent this issue, we propose a multi-step electrical tuning method. We show by simulations that the resonance frequency can be tuned by 0.008 Hz/mV even in the sub-1 Hz region. The small spring constant, however, reduces the shock robustness and dynamic range of the seismometer. To prevent this, we employ a force-balanced method in which the mass displacement is nulled by the feedback force. We show that the displacement can be obtained from the voltage that generates the feedback force.

Keywords: MEMS; seismometer; resonance frequency; force-balanced; electrical tuning

Citation: Wu, J.; Maekoba, H.; Parent, A.; Ikehashi, T. A Sub-1 Hz Resonance Frequency Resonator Enabled by Multi-Step Tuning for Micro-Seismometer. *Micromachines* **2022**, *13*, 63. https://doi.org/10.3390/mi13010063

Academic Editors: Aiqun Liu and Ion Stiharu

Received: 22 November 2021
Accepted: 28 December 2021
Published: 30 December 2021

Publisher's Note: MDPI stays neutral with regard to jurisdictional claims in published maps and institutional affiliations.

Copyright: © 2021 by the authors. Licensee MDPI, Basel, Switzerland. This article is an open access article distributed under the terms and conditions of the Creative Commons Attribution (CC BY) license (https://creativecommons.org/licenses/by/4.0/).

1. Introduction

A seismometer is a sensor that detects ground motions [1]. Mechanical seismometers adopt a mass-spring-damper system with a low resonance frequency so that the proof mass behaves as a fixed point relative to the ground. To achieve a resonance frequency of about 1 Hz, a kg-level heavy proof mass is usually used [2]. But the large mass and size is not suited for IoT applications that require compact seismometers [3].

Recently, mainly in the field of gravimeters, low resonance frequency MEMS structures are reported, as summarized in Table 1. In the case of Middlemiss' gravimeter, which has a similar structure to a seismometer, the resonance frequency of 2.3 Hz was achieved by an ultra-small spring constant composed of two kinds of mechanical spring, one of them having a negative spring constant [4].

Table 1. Comparison of the resonance frequencies of conventional works and this work.

Device	Proof Mass	Resonance Frequency
Middlemiss, R. [4]	13.64 mg	2.3 Hz
Tang, S. [5]	460 mg	3.1 Hz
Pike, W. T. [6,7]	400 mg	6 Hz
Wu, W. [8]	310 mg	14 Hz
Krishnamoort, U. [9]	33.6 mg	36 Hz
This work	24 mg	0.39 Hz

This paper aims to extend the approach to make a MEMS resonator with sub-1 Hz resonance frequency. Our final goal is to make a compact MEMS seismometer that can be used as an IoT sensor node. To achieve the small resonance frequency, we introduce an

electrically tunable negative spring constant enabled by parallel plate electrodes. Compared with the conventional method, electrical tunability has three advantages: (i) cancellation of process variation of spring constant, (ii) compensation of temperature dependence of spring constant, and (iii) yield improvement during fabrication and handling. The last point is attained by the larger spring constant of the power-off state, i.e., when no voltage is applied to the electrodes.

Electrical tuning of a resonance frequency is a well-known method [10,11]. However, making near zero resonance frequency is by no means easy, since the frequency shift Δf induced by a voltage shift ΔV will become very large when the spring constant k becomes small. This is due to the fact that $df/dV \propto 1/\sqrt{k}$. To resolve this issue, we introduce a multi-step electrical tuning method. We show that Δf can be made small enough even for the small spring constant.

The small spring constant, however, brings about some drawbacks. One is the reduction of shock robustness and the other is the decrease in dynamic range when applied to a seismometer. To circumvent these issues, we employ a force-balanced system. Namely, the displacement of the mass is sensed, and then a feedback force is generated based on the result, to cancel the displacement. Force-balanced methods have already been adopted in seismometers [12], but our system enables minimizing the size, since it only uses electrostatic forces.

2. Design

2.1. Electrically Tunable Spring

In a spring-mass system of spring constant k and mass m, the resonance frequency is given by

$$f = \frac{1}{2\pi}\sqrt{\frac{k}{m}}. \tag{1}$$

This formula indicates that small resonance frequency can be attained by small k even for small m. To account for process variations and robustness during the fabrication, it would be advantageous to attain the small k by electrical tuning [13]. A schematic of this electrically tunable spring is shown in Figure 1a. The total spring k is composed of mechanical spring k_m and parallel plate electrodes. Due to the symmetry of the electrode structure, attractive forces occur at both sides of the fixed electrodes. Noting that the force magnitude is proportional to V^2, the electrostatic force is written as $F_e = \alpha V^2 x$, with α being a constant. This implies that the electrostatic force can be regarded as a spring force with a negative spring constant, namely, $F_e = -k_e x$ with $k_e = -\alpha V^2 (< 0)$. The total spring constant thus becomes the sum of the two springs, $k = k_m + k_e$, and it can be tuned by the voltage V. Electrical short between the electrodes can be avoided by introducing stoppers, as in Figure 1a. As shown in Figure 1b, there are two points that can make zero k. The resonance frequency of this mechanical system shown in Figure 1a is

$$f = \frac{1}{2\pi}\sqrt{\frac{k_m - \alpha V^2}{m}}. \tag{2}$$

If the voltage is changed as $V \to V + \Delta V$, the frequency will change as

$$f' = f + \frac{df}{dV}\Delta V, \tag{3}$$

where

$$\frac{df}{dV} = -\frac{\alpha V}{2\pi\sqrt{m(k_m - \alpha V^2)}} \approx -\frac{k_m}{k}\cdot\frac{f}{V}. \tag{4}$$

This expression implies that as k becomes smaller, df/dV becomes larger, and it will become more difficult to fine-tune the frequency. For example, to attain a resonance frequency of 1 Hz with a 10 mg proof mass, the spring constant k should be as small as 4×10^{-4} N/m. If we further assume $k_m = 4$ N/m and $V = 10$ V, we obtain $|df/dV| = 1000$ Hz/V. Thus,

a small voltage fluctuation will lead to a large shift in the resonance frequency. This is the difficulty that needs to be resolved in order to attain $f < 1$ Hz.

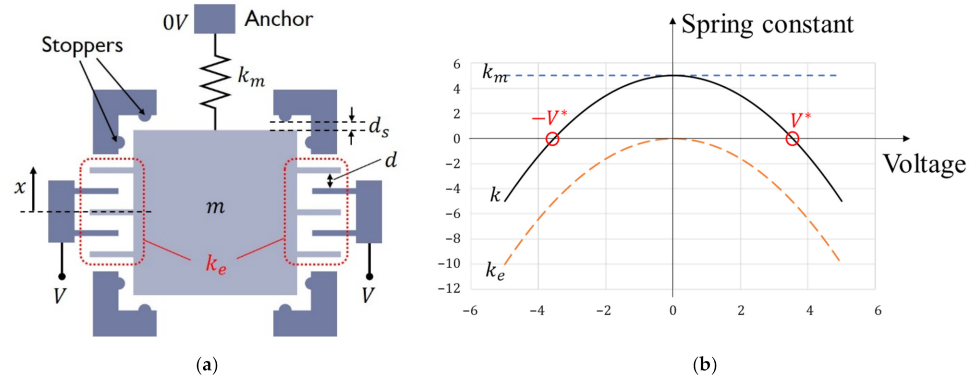

Figure 1. The basic principle of composite springs: (a) Schematic of seismometer structure. Total spring k is given by a sum of mechanical spring k_m and electrical spring $k_e (\propto V^2)$. Stoppers with gap d_s which is smaller than the electrode gap d, can prevent electrical short. (b) Behaviors of total spring $k = k_m + k_e$.

2.2. Multi-Step Electrical Tuning Method

To overcome the difficulty of fine-tuning, we employ a multi-step tuning method. In this method, we introduce three kinds of parallel plate electrodes to which different voltages can be applied. The frequency is then expressed as

$$f = \frac{1}{2\pi}\sqrt{\frac{k_m - \alpha_1 V_1^2 - \alpha_2 V_2^2 - \alpha_3 V_3^2}{m}}\,, \tag{5}$$

where V_i's are three independent voltages and α_i's are coefficients determined by electrode size. In terms of vacuum permittivity ε_0, electrode gap d and overlap area of i-th electrode A_i $(i = 1, 2, 3)$, the coefficient α_i is written as $\alpha_i = 2\varepsilon_0 A_i / d^3$. The frequency change Δf induced by the voltage change $\Delta V_1,\ \Delta V_2,\ \Delta V_3$ is written as

$$\Delta f = \frac{\partial f}{\partial V_1}\Delta V_1 + \frac{\partial f}{\partial V_2}\Delta V_2 + \frac{\partial f}{\partial V_3}\Delta V_3\,, \tag{6}$$

where

$$\frac{\partial f}{\partial V_i} = -\frac{\alpha_i V_i}{2\pi\sqrt{m(k_m - \alpha_1 V_1^2 - \alpha_2 V_2^2 - \alpha_3 V_3^2)}}. \tag{7}$$

If we set a condition $\alpha_1 \gg \alpha_2 \gg \alpha_3$ which can be attained by changing the electrode area A_i, we get

$$\left|\frac{\partial f}{\partial V_1}\right| \gg \left|\frac{\partial f}{\partial V_2}\right| \gg \left|\frac{\partial f}{\partial V_3}\right|. \tag{8}$$

This suggests that we can fine-tune the frequency by optimizing the voltages $V_1,\ V_2, V_3$ in this order. A practical method of multi-step tuning is depicted in Figure 2 and the tuning flow is shown in Figure 3. In this method, we stop the tuning of the first step before the slope $|df/dV|$ goes to infinity and start tuning of the second step. Similarly, we stop the second tuning before the slope goes to infinity and move on to the third step. By repeating this procedure, a small resonance frequency can be attained with reasonably small $|df/dV|$, which implies availability of fine frequency tuning. The number of tuning steps can be increased depending on the target frequency.

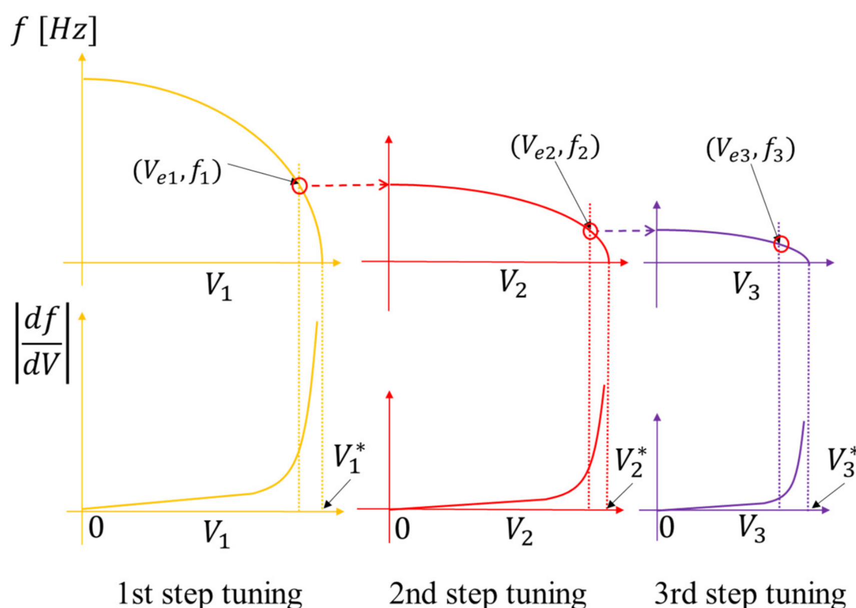

Figure 2. The basic principle of multi-step electrical tuning. In the 1st, 2nd, 3rd step tunings, frequencies will become 0 at V_1^*, V_2^*, V_3^*, respectively, and $|df/dV|$ goes to infinity at those voltages. Voltages V_{e1}, V_{e2}, V_{e3} are voltages slightly smaller than V_1^*, V_2^*, V_3^*.

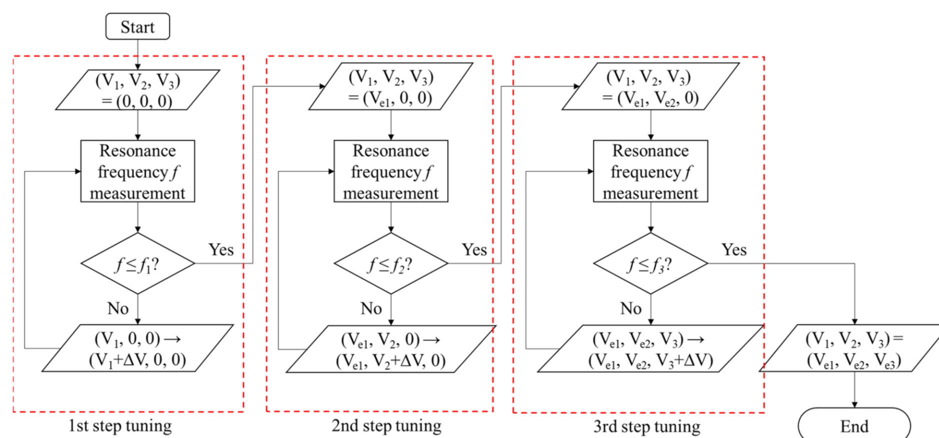

Figure 3. The flow chart of multi-step electrical tuning. Voltages V_1, V_2, V_3 are the voltages applied to 1st, 2nd, 3rd step tuning electrodes, respectively. And f_1, f_2, f_3 are the target resonance frequencies of each step. We set $f_1 = 8.0$ Hz, $f_2 = 1.9$ Hz, $f_3 = 0.4$ Hz for our resonator.

2.3. Seismometer Structure

The mechanical structure of our seismometer is shown in Figure 4. This structure can be fabricated by applying deep reactive ion etching (DRIE) to a silicon layer. Three sets of electrical springs, namely 1st, 2nd and 3rd electrical springs, are formed by symmetrical parallel plate electrodes. We also have position sensors and actuators composed of asymmetric parallel plate electrodes, which are used in the force-balanced system. The main dimensions are provided in Table 2.

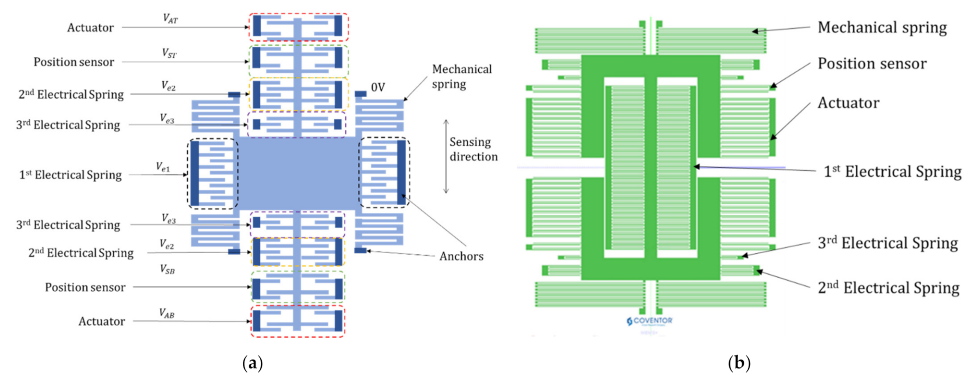

Figure 4. (**a**) Schematic of seismometer structure. (**b**) Top view of the seismometer layout used in a FEM simulator *MEMS+*.

Table 2. Dimensions of the seismometer.

Properties	Value	Unit
Si layer thickness	500	µm
Proof mass weight	24	mg
1st electrical spring finger length	1000	µm
1st electrical spring finger number	2 × 50	-
2nd electrical spring finger length	1000	µm
2nd electrical spring finger number	2 × 6	-
3rd electrical spring finger length	500	µm
Position sensor finger length	2 × 2	-
Position sensor finger number	1500	µm
Actuator finger length	2 × 2 × 2	-
Actuator finger number	1500	µm
Minimum gap of electrodes	2 × 2 × 13	-

2.4. Fabrication

Figure 5 shows a schematic fabrication process of our device. Firstly, recess patterns were made on a glass wafer. Then the wafer is anodic bonded to a silicon wafer. Finally, through silicon DRIE is done to make the movable portion.

Figure 5. Schematic fabrication process. Through silicon DRIE is applied to the silicon layer of the bonded wafer. The minimum gap of the silicon layer is 25 µm to attain an aspect ratio of 20.

2.5. Demonstration of Multi-Step Tuning

We are now in a position to demonstrate the fine-tuning procedure for the seismometer. To simulate the device performance, Coventor's multi-physics simulation tool, *MEMS+*® ,is employed [14]. Past studies proved *MEMS+* accurately predicts experimental electrostatic softening for manufactured gyroscopes [11,15]. The top view of the *MEMS+* simulated model is shown in Figure 4b. Firstly, when the three voltages V_1, V_2, V_3 are set to zero, the resonance frequency of the sensing direction was 90.3 Hz. Resonance frequencies of other modes are much higher than this value due to larger spring constants.

In the first step tuning, voltage V_1 is optimized with $V_2 = V_3 = 0$. As shown in Figure 6, the resonance frequency f will decrease with increasing V_1. If V_1 is changed with the 10 mV step, the resonance frequency f becomes minimum when V_1 is 12.220 V $\equiv V_1^*$,

as shown in the inserted figure. However, as indicated in Figure 6b, the frequency slope $|\partial f/\partial V_1|$ will become infinite as V_1 approaches to V_1^*. This indicates that fine frequency tuning is not possible at the vicinity of the V_1 that minimizes f.

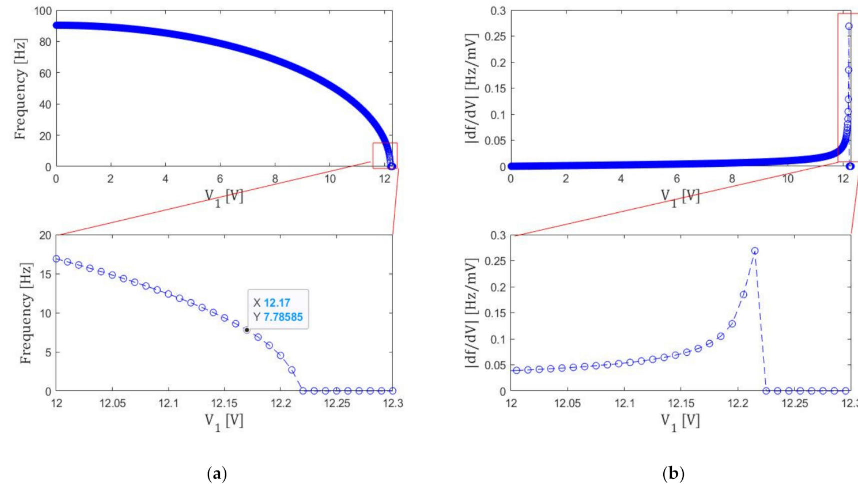

Figure 6. (a) Voltage V_1 dependence of the resonance frequency f. (b) Its derivative $|\partial f/\partial V_1|$.

Based on the flow chart of Figure 3, we stop the 1st step tuning when the resonance frequency becomes smaller than 8.0 Hz. As a result, we find that V_1 becomes 12.17 V, which is defined as V_{e1}. At this V_{e1}, frequency resolution can be made smaller than 0.1 Hz/mV. The resonance frequency at this voltage is 7.8 Hz and the spring constant is 0.157 N/m.

We apply the second step tuning to this state. The results are shown in Figure 7. The 2nd step tuning is done until the resonance frequency becomes smaller than 1.9 Hz. Then we find $V_2 = 2.98\ V \equiv V_{e2}$. Though the resonance frequency can be made smaller than 1 Hz in this step, we go to the next step to stabilize the resonance frequency against voltage fluctuations.

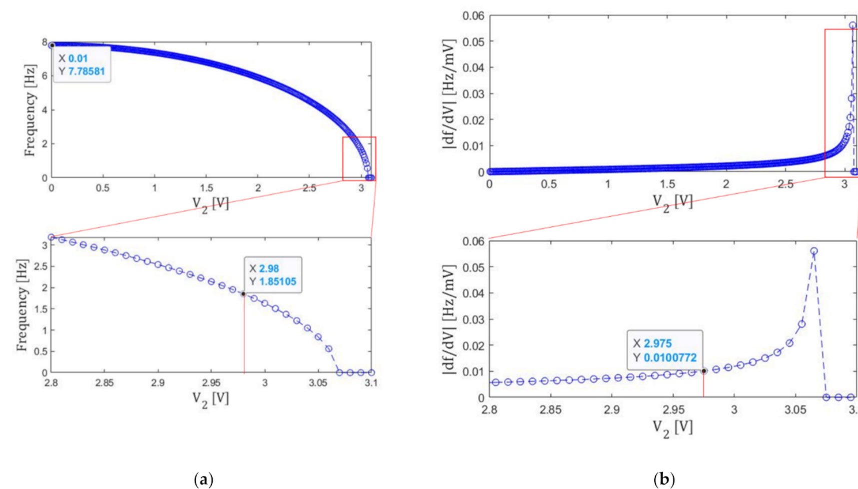

Figure 7. (a) Voltage V_2 dependence of the resonance frequency f. (b) Its derivative $|\partial f/\partial V_2|$.

At this V_{e2}, due to the smaller electrode area, the slope $|\partial f/\partial V_2|$ can be made smaller than 0.01 Hz/mV. The resonance frequency after this step is 1.85 Hz.

Finally, 3rd step tuning is applied to this state. The results are shown in Figure 8. The 3rd step tuning is done until the resonance frequency becomes smaller than 0.4 Hz. Then we find $V_3 = 1.77\ V \equiv V_{e3}$. The slope $|\partial f/\partial V_3|$ can now become smaller than 0.008 Hz/mV.

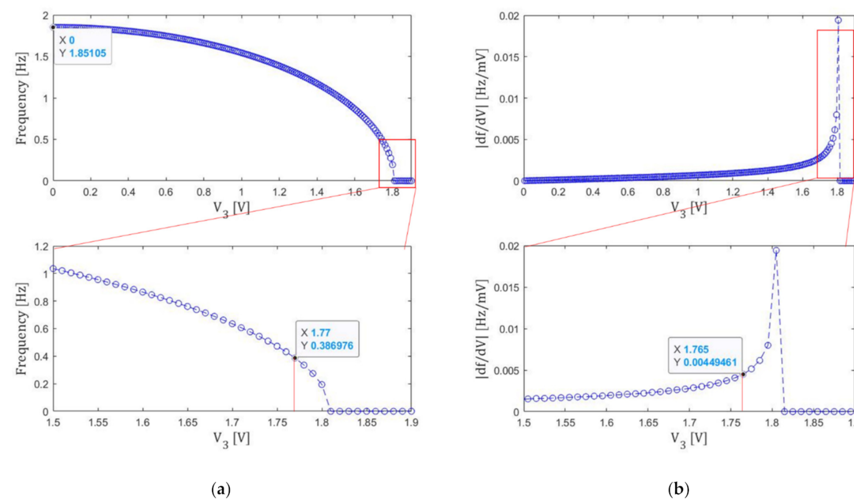

(**a**) (**b**)

Figure 8. (a) Voltage V_3 dependence of the resonance frequency f. (b) Its derivative $|\partial f/\partial V_3|$.

To summarize, we have set $V_{e1} = 12.17$ V, $V_{e2} = 2.98$ V, and $V_{e3} = 1.77$ V. The resulting resonance frequency was found to be 0.39 Hz. Note that the size increase caused by the second and the third tuning is small since their electrode areas are far smaller than the first one.

2.6. Force-Balance System

The small spring constant we have achieved has an issue with respect to the shock immunity and dynamic range of the sensor. To circumvent this, we introduce a force-balanced approach. The concept of the force-balanced system is shown in Figure 9a. When a displacement occurs due to an external force, the position sensor detects the displacement, and a force will be applied to nullify the displacement. The displacement can be known from the voltage required to cancel the displacement.

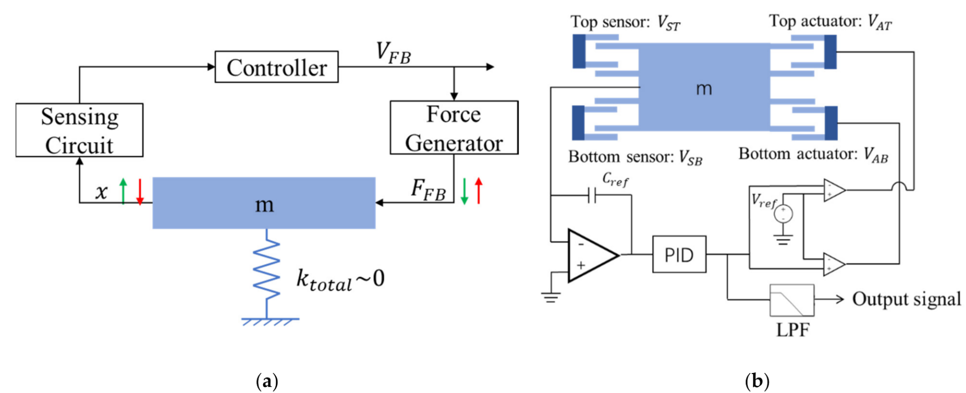

(**a**) (**b**)

Figure 9. (**a**) Basic concept of force-balance method. (**b**) Circuit block diagram of seismometer.

This kind of force-balanced system is already adopted in seismometers. The conventional system, however, uses magnetic force that calls for many components and bulky coil [12]. On the other hand, the present system can be made more compact since it only uses electrostatic force, and therefore the whole mechanical system can be embedded in a single chip.

A schematic block diagram of our force-balanced system is shown in Figure 9b. A pair of asymmetrical gap electrodes are used for the position sensor and actuators. To minimize the offset and overshooting/undershooting of the output voltage V_{FB}, we introduce a PID controller. Based on the voltage V_{FB}, upward and downward forces are generated by the top and bottom actuators.

We have also undertaken multi-domain simulation of the device coupled to the control system. Here, the MEMS+ model is employed directly in MathWorks Simulink together with other system blocks to model the control loop. The block diagram of the total system is shown in Figure 10. The target frequency range of our seismometer is 0.01 Hz to 100 Hz. To confirm the response of our system, we carried out simulations at the typical frequency 5 Hz and the maximum frequency 100 Hz. The simulation results are shown in Figures 11 and 12. The results show that the input acceleration is correctly reflected in the output voltage and at the same time, the displacement is canceled. The cancellation of the displacement implies that it can also eliminate nonlinearities that occur at large displacements. The nonlinearity originates from both mechanical spring and electrostatic forces.

The open-loop sensitivity, namely the sensitivity when the force-balanced system is turned off, is given by

$$\frac{\Delta C}{\Delta g} = \frac{\Delta C}{\Delta x} \cdot \frac{\Delta x}{\Delta g} = \frac{\Delta C}{\Delta x} \cdot \frac{1}{(2\pi f)^2}, \quad (9)$$

where f is the resonance frequency. Using the simulated value for $\Delta C/\Delta x$ and 0.39 Hz for f, we find that the sensitivity becomes 13.9 nF/(m/s^2). When the force-balance system is turned on, the displacement is nulled, and the sensitivity becomes 2.0 V/(m/s^2).

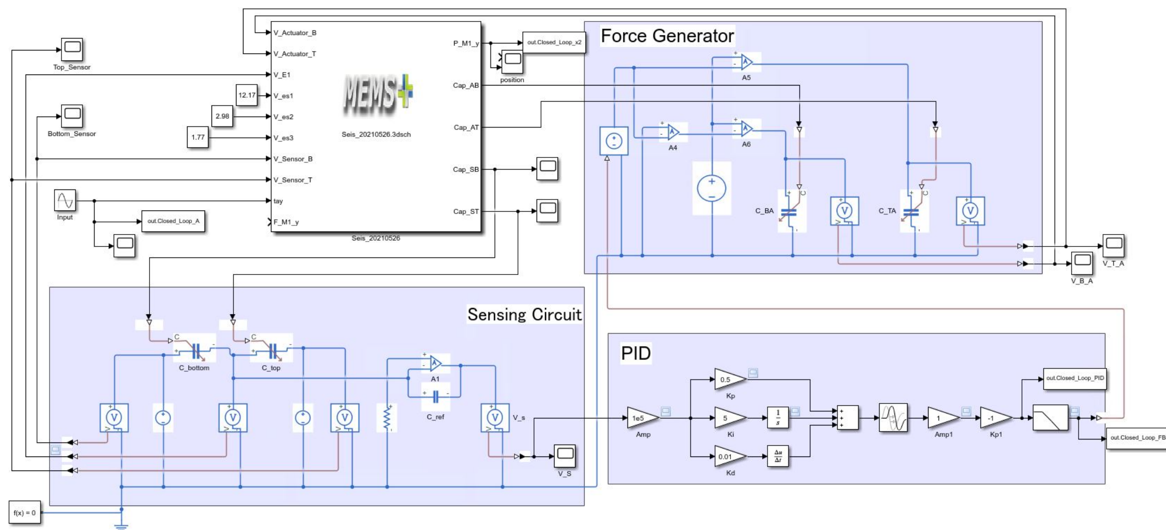

Figure 10. Block diagram of the multi-domain simulation.

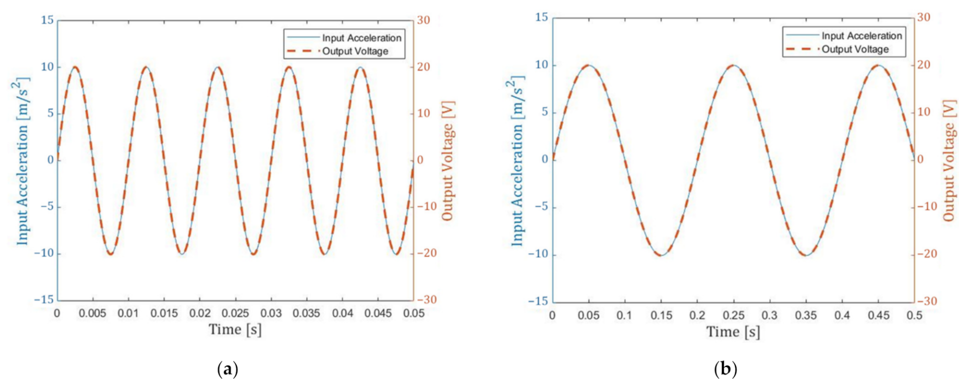

(**a**) (**b**)

Figure 11. Simulation results of different acceleration input frequencies (**a**) 100 Hz (maximum frequency); (**b**) 5 Hz (typical frequency). The solid line corresponds to the input acceleration, and the dashed line corresponds to the output voltage. Matching of the two curves implies that the system can respond to the input accelerations. Results for lower frequencies are not shown because catching up to the input will become much easier.

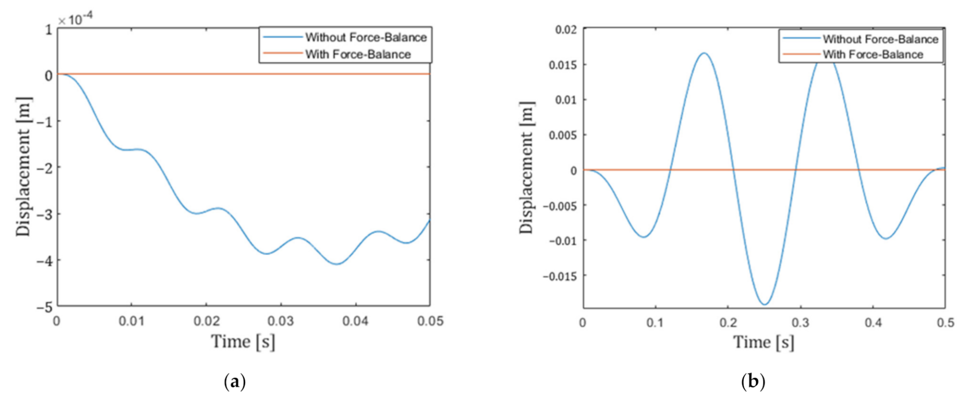

Figure 12. Simulation results of different acceleration input frequencies (**a**) 100 Hz; (**b**) 5 Hz. The *x*-axis is the time; the *y*-axis is displacements of the proof mass in different cases. The displacement becomes smaller for the higher frequency due to the small resonance frequency of 0.39 Hz.

3. Conclusions

In this paper, a design methodology of a resonator with ultra-small resonance frequency is presented. Using the proposed three-step electrical tuning, the total spring constant can be easily tuned, and the resonance frequency of the resonator can be tuned to 0.39 Hz and at 0.008 Hz/mV level. A force-balance method that can attain shock robustness and dynamic range enhancement is also proposed and verified by simulation. The primary goal of this study is to attain a MEMS seismometer. However, the design scheme presented here can also be applied to other sensors that call for ultra-small resonance frequencies, such as gravimeters and vibration sensors.

Author Contributions: Conceptualization, J.W. and T.I.; methodology, J.W. and H.M.; software, J.W., H.M. and A.P.; validation, H.M., A.P. and T.I.; formal analysis, J.W. and T.I.; investigation, J.W., H.M. and A.P.; resources, H.M. and A.P.; data curation, H.M., A.P. and T.I.; writing—original draft preparation, J.W.; writing—review and editing, H.M., A.P. and T.I.; visualization, J.W. and T.I.; supervision, A.P. and T.I.; project administration, T.I.; funding acquisition, T.I. All authors have read and agreed to the published version of the manuscript.

Funding: This research was funded by JSPS KAKENHI grant number JP21K04855.

Acknowledgments: This work was supported by JSPS KAKENHI Grant Number JP21K04855.

Conflicts of Interest: The authors declare no conflict of interest.

References

1. Hou, Y.; Jiao, R.; Yu, H. MEMS based geophones and seismometers. *Sens. Actuators A Phys.* **2021**, *318*, 112498. [CrossRef]
2. Havskov, J.; Alguaci, G. *Instrumentation in Earthquake Seismology*; Springer: Dordrecht, The Netherlands, 2016; pp. 94–96.
3. Lee, J.; Khan, I.; Choi, S.; Kwon, Y.-W. A Smart IoT Device for Detecting and Responding to Earthquakes. *Electronics* **2019**, *8*, 1546. [CrossRef]
4. Middlemiss, R.; Samarelli, A.; Paul, D.; Hough, J.; Rowan, S.; Hammond, G.D. Measurement of the Earth tides with a MEMS gravimeter. *Nature* **2016**, *531*, 614–617. [CrossRef] [PubMed]
5. Tang, S.; Liu, H.; Yan, S.; Xu, X.; Wu, W.; Fan, J.; Liu, J.; Hu, C.; Tu, L. A high-sensitivity MEMS gravimeter with a large dynamic range. *Microsyst. Nanoeng.* **2019**, *5*, 45. [CrossRef] [PubMed]
6. Pike, W.T.; Delahunty, A.K.; Mukherjee, A.; Dou, G.; Liu, H.; Calcutt, S.; Standley, I.M. A self-levelling nano-g silicon seismometer. In Proceedings of the SENSORS, 2014 IEEE, Valencia, Spain, 2–5 November 2014; pp. 1599–1602.
7. Pike, W.T.; Standley, I.M.; Calcutt, S.B.; Mukherjee, A. A broad-band silicon microseismometer with 0.25 NG/rtHz performance. In Proceedings of the 2018 IEEE Micro Electro Mechanical Systems (MEMS), Belfast, Ireland, 21–25 January 2018; pp. 113–116.
8. Wu, W.; Liu, J.; Fan, J.; Peng, D.; Liu, H.; Tu, L. A nano-g micromachined seismic sensor for levelling-free measurements. *Sens. Actuators A Phys.* **2018**, *280*, 238–244. [CrossRef]
9. Krishnamoorthy, U.; Olsson, R.H.; Bogart, G.R.; Baker, M.S.; Carr, D.W.; Swiler, T.P.; Clews, P.J. In-plane MEMS-based nano-g accelerometer with sub-wavelength optical resonant sensor. *Sens. Actuators A Phys.* **2008**, *145–146*, 283–290. [CrossRef]
10. Lee, M.; Hwang, J.G.; Jahng, J.; Kim, Q.; Noh, H.; An, S.; Jhe, W. Electrical tuning of mechanical characteristics in qPlus sensor: Active Q and resonance frequency control. *J. Appl. Phys.* **2016**, *120*, 074503. [CrossRef]

11. Parent, A.; Krust, A.; Lorenz, G.; Favorskiy, I.; Piirainen, T. Efficient nonlinear Simulink models of MEMS gyroscopes generated with a novel model order reduction method. In Proceedings of the 2015 Transducers—2015 18th International Conference on Solid-State Sensors, Actuators and Microsystems (TRANSDUCERS), Anchorage, AK, USA, 21–25 June 2015; pp. 2184–2187.
12. Wielandt, E.; Streckeisen, G. The leaf-spring seismometer: Design and performance. *Bull. Seismol. Soc. Am.* **1982**, *72*, 2349–2367.
13. Chen, Z.; Ikehashi, T. A Mode Localized Tilt Sensor with Ultra-Small Stiffness Spring. In Proceedings of the Microprocesses and Nanotechnology Conference (MNC), Osaka, Japan, 9–12 November 2020.
14. MEMS+®. Available online: https://www.coventor.com/products/coventormp/mems-plus/ (accessed on 29 December 2021).
15. Parent, A.; Krust, A.; Lorenz, G.; Favorskiy, I.; Piirainen, T. A novel model order reduction approach for generating efficient nonlinear Verilog-A models of mems gyroscopes. In Proceedings of the 2015 IEEE International Symposium on Inertial Sensors and Systems (ISISS), Hapuna Beach, HI, USA, 23–26 March 2015; pp. 1–4.